





Article

Toledoite, TiFeSi, a New Mineral from Inclusions in Corundum Xenocrysts from Mount Carmel, Israel

Chi Ma ^{1,*}, Fernando Cámara ², Luca Bindi ³ and William L. Griffin ^{4,*}¹ Division of Geological and Planetary Sciences, California Institute of Technology, Pasadena, CA 91125, USA² Dipartimento di Scienze della Terra “A. Desio”, Università degli Studi di Milano, Via Mangiagalli 34, I-20133 Milan, Italy; fernando.camara@unimi.it³ Dipartimento di Scienze della Terra, Università degli Studi di Firenze, Via La Pira 4, I-50121 Florence, Italy; luca.bindi@unifi.it⁴ ARC Centre of Excellence for Core to Crust Fluid Systems and GEMOC, Earth and Environmental Sciences, Macquarie University, Macquarie Park, NSW 2109, Australia

* Correspondence: chima@caltech.edu (C.M.); bill.griffin@mq.edu.au (W.L.G.)

Abstract: During our nanomineralogical investigation of melt inclusions in corundum xenocrysts from the Mount Carmel area, Israel, seven new oxide and alloy minerals have been discovered since 2021. Herein, we report toledoite (TiFeSi; IMA 2022-036), a new alloy mineral. Toledoite occurs as irregular crystals 2–16 μm in size, with gupeiite (Fe_3Si), jingsuiite (TiB_2), ziroite (ZrO_2), osbornite (TiN), xifengite (Fe_5Si_3), and naquite (FeSi) in corundum Grain WG1124E-1. Toledoite has an empirical formula $(\text{Ti}_{0.83}\text{Cr}_{0.07}\text{Mn}_{0.06}\text{V}_{0.02})(\text{Fe}_{0.96}\text{Mn}_{0.04})(\text{Si}_{0.99}\text{P}_{0.04})$ and an orthorhombic *Ima2* TiFeSi-type structure with the following cell parameters: $a = 7.00(1) \text{ \AA}$, $b = 10.83(1) \text{ \AA}$, $c = 6.29(1) \text{ \AA}$, $V = 477(1) \text{ \AA}^3$, $Z = 12$. Toledoite is a high-temperature alloy phase, formed under extremely reduced conditions in melt pockets in corundum xenocrysts derived from the upper mantle beneath Mount Carmel in Israel. The name was given in honor of Vered Toledo, of Shefa Gems Ltd. for her support and for providing corundum xenocrysts from the Mount Carmel region for this investigation of new minerals.

Keywords: toledoite; TiFeSi; new mineral; corundum; Mount Carmel; Israel

Citation: Ma, C.; Cámara, F.; Bindi, L.; Griffin, W.L. Toledoite, TiFeSi, a New Mineral from Inclusions in Corundum Xenocrysts from Mount Carmel, Israel. *Crystals* **2024**, *14*, 96. <https://doi.org/10.3390/cryst14010096>

Academic Editors: Per-Lennart Larsson and Vladislav V. Gurzhiy

Received: 17 November 2023

Revised: 18 January 2024

Accepted: 19 January 2024

Published: 21 January 2024



Copyright: © 2024 by the authors. Licensee MDPI, Basel, Switzerland. This article is an open access article distributed under the terms and conditions of the Creative Commons Attribution (CC BY) license (<https://creativecommons.org/licenses/by/4.0/>).

1. Introduction

Mineral assemblages containing super-reduced phases (formed in low oxygen fugacities below the iron–wüstite buffer) are commonly associated with explosive volcanic events. These include kimberlites, alkali basalts, and tholeiitic basalts, as well as in ophiolites linked to deep subduction along continental plate margins [1–4]. In volcanic localities, super-reduced phases are frequently found as inclusions within xenoliths composed of corundum aggregates. The relationships between these different phases within melt inclusions have been crucial in comprehending the genesis of super-reduced magma–fluid systems [4].

We have studied the mineralogy of crystals down to nanoscale in melt inclusions in corundum xenocrysts coming from volcanic centers and associated alluvial deposits in the Mount Carmel area, Israel. Since 2021, we have identified seven IMA-approved new minerals: griffinite (Al_2TiO_5), magnéliite ($\text{Ti}^{3+}_2\text{Ti}^{4+}_2\text{O}_7$), ziroite (ZrO_2), sassite ($\text{Ti}^{3+}_2\text{Ti}^{4+}\text{O}_5$), mizraite-(Ce) ($\text{Ce}(\text{Al}_{11}\text{Mg})\text{O}_{19}$), toledoite (TiFeSi), and yeite (TiSi) [5]. Reported here is toledoite; we will also provide additional information on the origin and stability of reduced high-temperature minerals from the upper mantle.

Natural iron silicides are found as components of fulgurites, planetary materials, in meteorites and interstellar dust. For example, xifengite (Fe_5Si_3) is found with the reduced-oxide minerals tistarite (Ti_2O_3) and kaitianite ($\text{Ti}^{3+}_2\text{Ti}^{4+}\text{O}_5$) in the matrix of the Allende meteorite—the largest known carbonaceous chondrite, which formed under reducing conditions in the solar nebula [6].

Toledoite (IMA 2022-036) is a new mineral. Its chemical formula is TiFeSi , and it exhibits an *Ima2* TiFeSi -type structure. The name is in honor of Vered Toledo (b. 1968), of Shefa Gems Ltd. for her support and for providing corundum xenocrysts from the Mount Carmel region for this investigation of new minerals. The type of toledoite is included in corundum grain WG1124E-1, which is part of Mount Carmel mount WG1124E. The mount was deposited in the mineralogy collection of the Università degli Studi di Milano, Via Mangiagalli, 34 - 20133 Milano, Italy under registration number MCMGPG-H2021-006.

2. Materials and Methods

The samples of this study are corundum xenoliths found to occur in the pyroclastic ejecta coming from small cretaceous basaltic volcanoes exposed on Mount Carmel (Figure 1) and in placer gemstone deposits in the terraces of the Paleocene to Pleistocene proto-Kishon river. The modern Kishon River and its tributary Mizra river now drain Mount Carmel and the adjacent Yisre'el Valley, and the Kishon River enters the sea near Haifa in northern Israel. U-Pb dating of super-reduced minerals in the corundum aggregates [4] indicates that much of the xenolith material in the paleoterrace placer deposits was derived from Miocene to Paleocene basalts outcropping in the Yisre'el Valley.

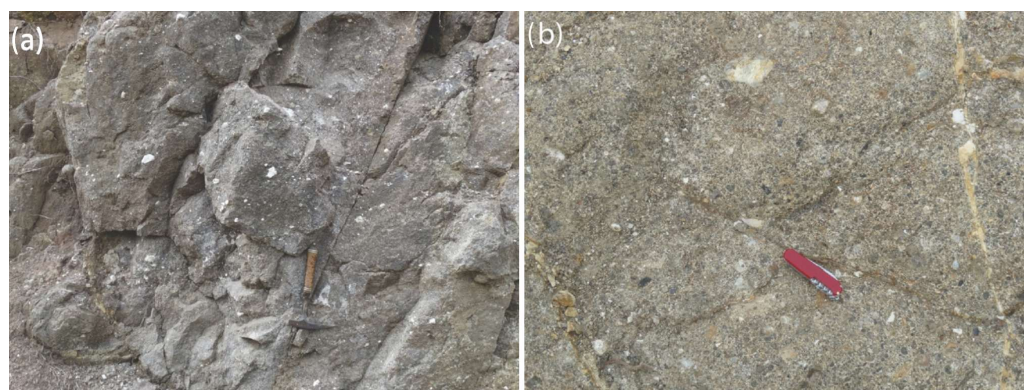


Figure 1. (a) Black massive pyroclastic rocks cropping out in Vent #1 of the Rakefet magmatic complex on Mount Carmel; a geological hammer used for scale. Country rock limestones are occasionally included as white clasts. (b) A closer view of massive pyroclastics in the Rakefet magmatic complex; a knife used for scale.

The studied grain was separated from a 400-tonne bulk sample of a basal paleo-placer deposit of the Paleocene–Pleistocene paleo-Kishon River (BS1124; coordinates: 35.106E/32.685N). The xenoliths can be described as aggregates of skeletal corundum crystals containing melt pockets in which the reduced mineral assemblages are found [4].

Recently, the genesis of the super-reduced phases has been the subject of discussion, with several authors arguing for an anthropogenic origin [7–11]. Unfortunately, the authors of these papers have chosen to ignore the extensive geological and geochemical evidence for the natural origin of the Mount Carmel xenolith material. This evidence has been summarized in detail in [12,13]. The latter reference presents U-Pb dating of carmelazite and other super-reduced phases in the corundum aggregates, which shows a pattern of age distribution (Paleocene to Miocene, Cretaceous and older) that is consistent with zircon dating [14] of the volcanic rocks thought to be the immediate sources of the super-reduced phases [5]. It is clear from these data, as well as the geological context, that the Mount Carmel material was not produced by human beings.

For the characterization of the sample, we used an electron probe microanalyzer (EPMA) and a field-emission scanning electron microscope (SEM) equipped with an X-ray energy-dispersive spectrometer (EDS) and a detector for electron backscatter diffraction (EBSD), which allowed us to characterize both the composition and the structure of toledoite and associated phases. The instruments used for these analyses were a ZEISS 1550VP Field-Emission SEM (ZEISS Group, Oberkochen, Germany) equipped with an Oxford X-Max

EDS, which was used for back-scatter electron (BSE) imaging and fast elemental analysis. For quantitative WDS elemental microanalyses of toledoite, we used a JEOL 8200 EPMA (JEOL Ltd., Tokyo, Japan) (15 kV and 10 nA, focused beam) interfaced with the Probe for EPMA program from Probe Software, Inc. (Eugene, OR, USA). The focused electron beam was ~150 nm in diameter. Quantitative WDS analyses were processed with the CITZAF matrix correction procedure. Analytical results are given in Table 1.

Table 1. EPMA analytical results (in wt%, n = 12) for toledoite.

Constituent	Mean	Range	SD	Probe Standard
Fe	40.47	39.92–41.17	0.37	Fe metal
Ti	29.94	29.39–30.84	0.47	Ti metal
Si	20.83	20.29–21.29	0.25	Si metal
Mn	3.96	3.69–4.14	0.11	Mn ₂ SiO ₄
Cr	2.73	2.54–2.91	0.10	Cr metal
V	0.77	0.71–0.85	0.04	V metal
P	0.82	0.71–1.24	0.17	GaP
Total	99.52			

Due to the small size of the crystal, conventional X-ray studies could not be carried out. Therefore, EBSD analyses at a submicrometer scale were carried out, as in other previous studies of new minerals [5], by using an HKL EBSD system mounted on the ZEISS 1550VP SEM. Operation conditions were 20 kV and 6 nA in focused-beam mode using a 70° tilted stage, and in variable-pressure mode (25 Pa). A single crystal of silicon was used for calibration of the EBSD system. Structural correspondence was obtained and cell constants were derived by matching the experimental EBSD patterns with those obtained from the structures of synthetic Ti-Fe-Si, Ti-Si, and Fe-Si phases available in the ICSD.

Because of the very small size of the crystals, the determination of most of the physical properties (optical, hardness, fracture, cleavage, habit, density, etc.) was impracticable without risking destruction of the material.

3. Results

Toledoite occurs with gupieite (Fe₃Si) [15], jingsuiite (TiB₂) [16], ziroite (ZrO₂) [5], osbornite (TiN) [17], xifengite (Fe₅Si₃) [15], and naquite (FeSi) [18] in melt inclusions in corundum grain WG1124E-1 (Figure 2). Ti-bearing xifengite and osbornite are also present in the Allende meteorite [6]. Other inclusions in this corundum grain contain an Allende-like Ti,Al,Zr-oxide [6], khamrabaevite (TiC), spinel, grossmanite-kushiroite-diopside, and Ce-silicate. Toledoite has been found as anhedral crystals (size: 2–16 μm). It is opaque and black in color.

Chemical data (Table 1—electron probe microanalyses) point to the empirical formula (based on three atoms' *pfu*) of (Ti_{0.83}Cr_{0.07}Mn_{0.06}V_{0.02})(Fe_{0.96}Mn_{0.04})(Si_{0.99}P_{0.04}). The simplified formula can be written as (Ti,Cr,Mn)(Fe,Mn)Si. The ideal formula is TiFeSi, which requires Ti 36.32, Fe 42.37, Si 21.31, and a total 100 wt%.

The EBSD patterns obtained for toledoite are best indexed by using the orthorhombic *Ima2* TiFeSi-type structure and match the cell known for synthetic TiFeSi [19] (Figure 3), with a mean angular deviation of 0.33–0.36°. The following cell parameters have been obtained: *a* = 7.00(1) Å, *b* = 10.83(1) Å, *c* = 6.29(1) Å, *V* = 477(1) Å³, *Z* = 12. A calculated density of 5.53 g·cm^{−3} is obtained by using the empirical formula and the unit cell volume estimated from EBSD data. Powder Cell version 2.4 was used to calculate X-ray powder diffraction data (Table 2, in Å for CuKα₁, Bragg–Brentano geometry) from the unit cell parameters reported above, the crystallographic data of synthetic TiFeSi [19], and the empirical formula.

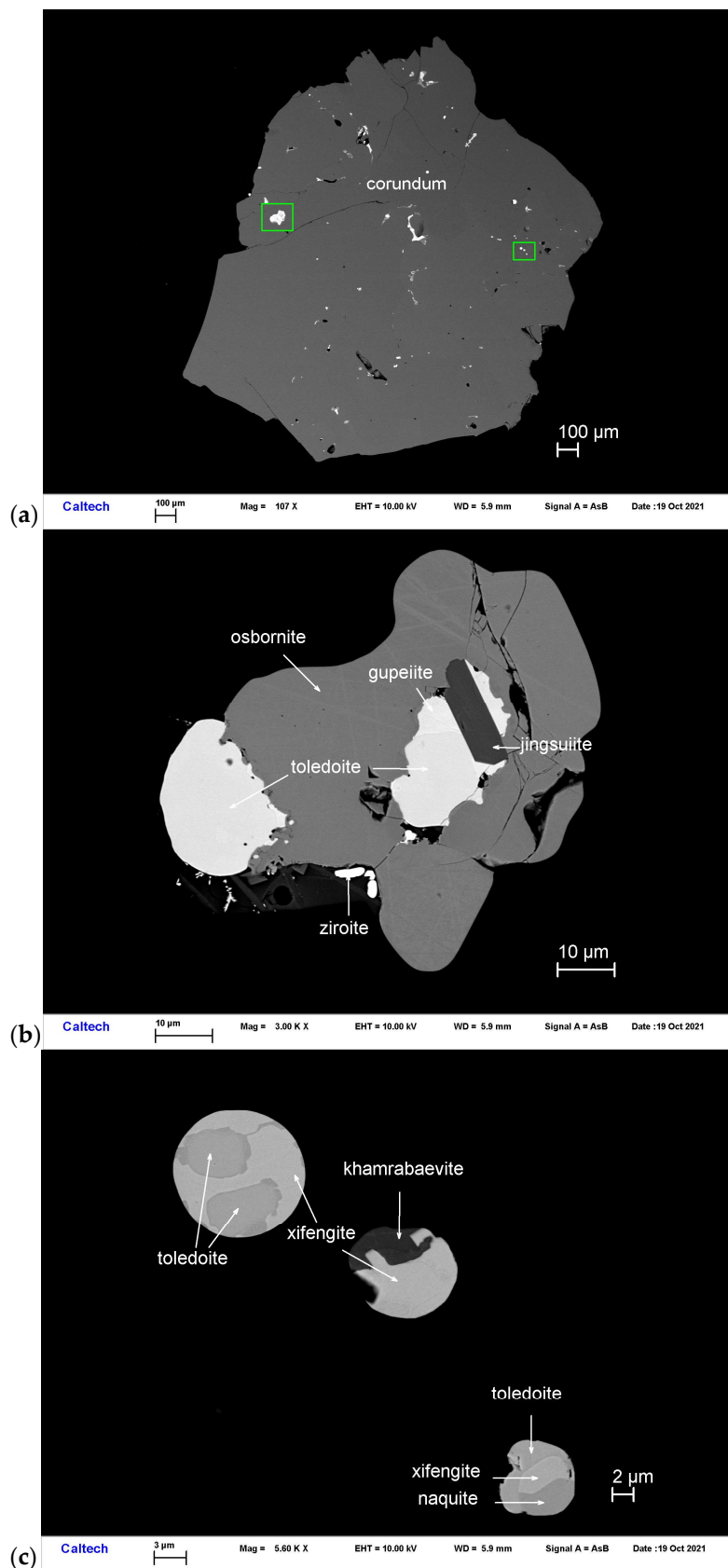


Figure 2. Back-scattered electron images showing toledoite (TiFeSi) in corundum grain WG1124E-1. The rectangular areas in (a) are enlarged in (b,c).

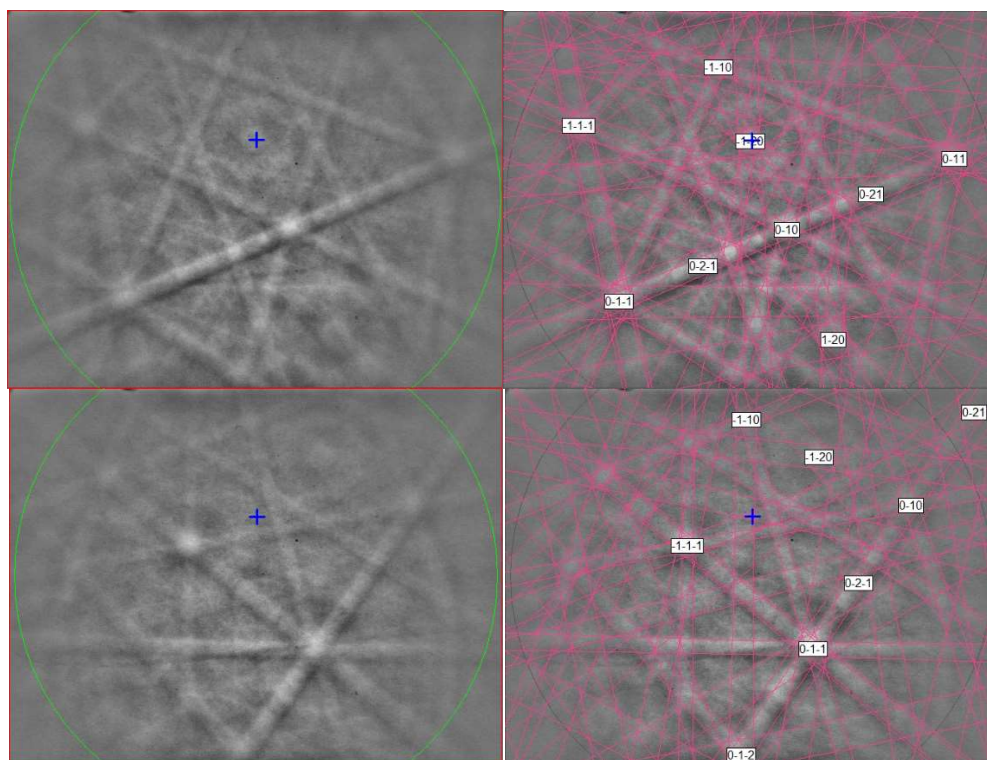


Figure 3. (left) EBSD patterns of two toledoite crystals in Figure 2, and (right) the patterns indexed with the *Ima2* TiFeSi-type structure. The blue cross is pattern center. The diffraction bands in the green circle were used for indexing.

Table 2. Calculated X-ray powder diffraction data for toledoite ($I_{rel} > 1$). The strongest lines in the powder X-ray diffraction pattern are in bold.

<i>h</i>	<i>k</i>	<i>l</i>	<i>d</i> [Å]	<i>I_{rel}</i>
1	1	0	5.8789	1
0	1	1	5.4392	6
0	2	0	5.4150	3
1	2	1	3.5402	1
2	0	0	3.5000	5
0	0	2	3.1450	3
0	3	1	3.1310	5
2	1	1	2.9433	7
2	2	0	2.9394	4
0	2	2	2.7196	3
0	4	0	2.7075	1
1	4	1	2.3434	1
2	0	2	2.3393	44
2	3	1	2.3335	100
3	1	0	2.2810	4
1	3	2	2.2460	3
2	2	2	2.1475	89
2	4	0	2.1415	38
1	5	0	2.0692	4
0	1	3	2.0585	36
0	4	2	2.0519	33
0	5	1	2.0480	34
3	2	1	2.0284	8
3	3	0	1.9596	2

Table 2. Cont.

<i>h</i>	<i>k</i>	<i>l</i>	<i>d</i> [Å]	<i>I</i> _{rel}
1	2	3	1.8831	2
3	1	2	1.8465	4
0	3	3	1.8131	17
0	6	0	1.8050	8
2	1	3	1.7743	12
2	4	2	1.7701	12
2	5	1	1.7676	11
4	0	0	1.7500	36
3	4	1	1.7016	1
1	6	1	1.6840	1
3	3	2	1.6632	2

In the structure of toledoite, each Fe atom forms four bonds with adjacent Si atoms creating layers of two different FeSi₄ distorted tetrahedra ($\langle Fe1-Si \rangle = 2.374 \text{ \AA}$, distortion parameter in the sense of [20], $D = 0.01342$, and $\langle Fe2-Si \rangle = 2.405 \text{ \AA}$, $D = 0.00628$) with Ti atoms present in the empty cavities between them (Figure 4a,b). Ti is five-fold coordinated with Si atoms, forming three different TiSi₅ distorted square pyramids ($\langle Ti1-Si \rangle = 2.606 \text{ \AA}$, $D = 0.02593$, $\langle Ti2-Si \rangle = 2.572 \text{ \AA}$, $D = 0.00459$ and $\langle Ti3-Si \rangle = 2.575 \text{ \AA}$, $D = 0.00620$) that share edges among them and with FeSi₄ tetrahedra. The FeSi₄ tetrahedra share edges and apexes, thus forming (Fe₆Si₁₄)_∞ chains extending along [100] (Figure 4c). The union of these chains by sharing apexes builds a three-dimensional framework. Toledoite has a very different structural topology than the other natural titanium ferro-silicide, zangboite (TiFeSi₂ [21]), found in Luobusha, Tibet, China. In zangboite, iron is bonded to 6 Si atoms in very distorted FeSi₆ octahedron ($\langle Fe1-Si \rangle = 2.3646 \text{ \AA}$, distortion parameter $D = 0.01009$, and $\langle Fe2-Si \rangle = 2.3854 \text{ \AA}$, distortion parameter $D = 0.02728$), while Ti is seven-fold coordinated with Si in distorted TiSi₇ capped octahedra ($\langle Ti1-Si \rangle = 2.691 \text{ \AA}$, distortion parameter $D = 0.01806$, and $\langle Ti2-Si \rangle = 2.6534 \text{ \AA}$, distortion parameter $D = 0.01397$). In zangboite, FeSi₆ octahedra share a face and edges and form three-octahedra-wide ribbons along [001], which share vertices with adjacent ribbons. The spaces among the ribbons are filled by TiSi₇-capped octahedra sharing faces.

Electron backscattering diffraction coupled with electron microprobe analyses allowed us to identify gupeiite—(Fe_{2.28}Mn_{0.28}Ti_{0.19}Cr_{0.15}V_{0.01})Si_{1.09}, xifengite—(Fe_{3.54}Ti_{0.60}Mn_{0.45}Cr_{0.25}V_{0.03})Si_{3.13}, and naquite—(Fe_{0.64}Ti_{0.27}Mn_{0.08}Cr_{0.07}V_{0.01})Si_{0.94} as associated phases.

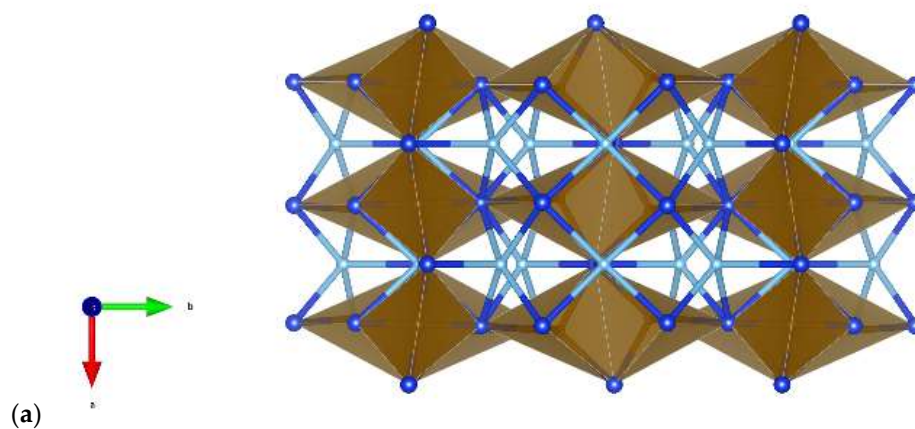


Figure 4. Cont.

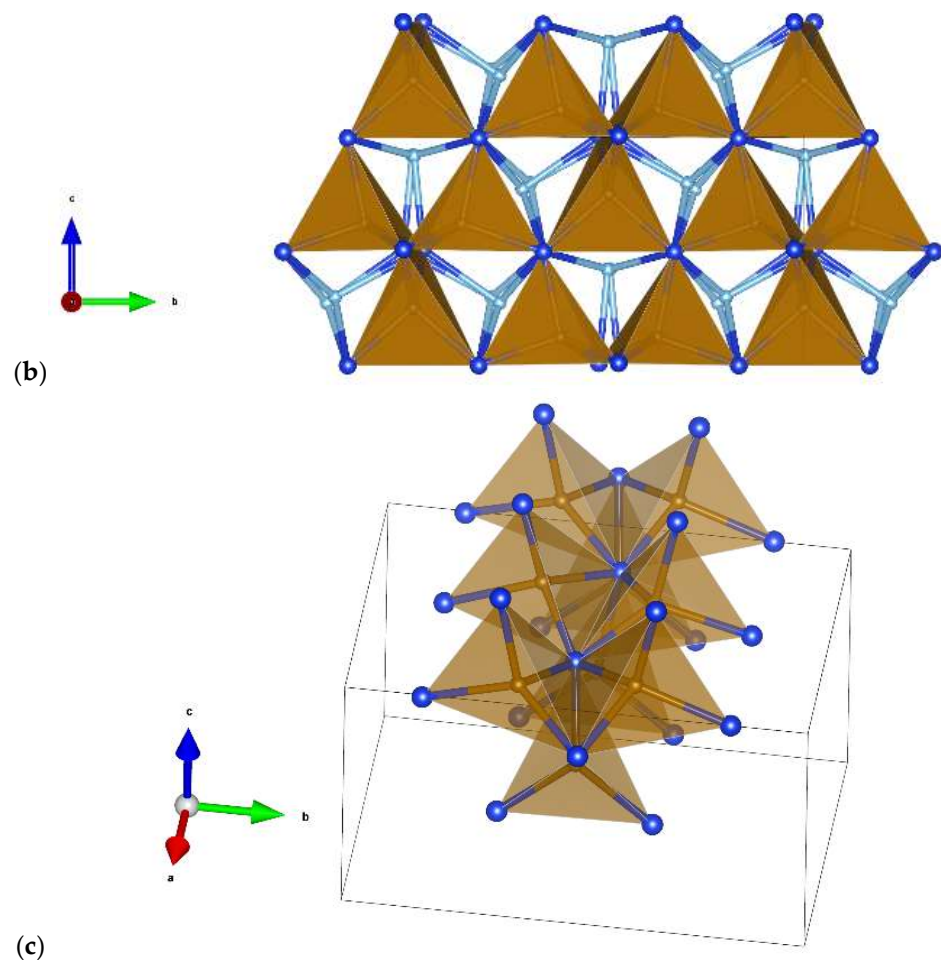


Figure 4. The structure of toledoite (using the atom coordinates published in [19]). FeSi_4 tetrahedra are in brown and TiSi_5 square pyramids are in cyan. Plots obtained using Vesta 3.0. [22]. (a) Projected down [001], (b) down [100], and (c) detail of the $(\text{Fe}_6\text{Si}_{14})_\infty$ chains extending along [100], in which the FeSi_4 tetrahedra share edges.

Toledoite is natural TiFeSi with an $Ima2$ TiFeSi -type structure. Synthetic TiFeSi is well known [19,23–25]. Toledoite is not related to other minerals to our knowledge. The structure is a superstructure of the hexagonal ordered Fe_2P -type [19]. Synthetic TiFeSi may also show the hexagonal $P-62m$ β -form polymorph ($a = 6.257(2)$, $c = 3.497(1)$ (Å), $V = 118.55(9)$ Å³ [24]), which is stable at high- T , but inverts to the orthorhombic phase after annealing at 1273 K for seven days.

4. Discussion

The alloy phases studied herein occur as inclusions in aggregates of corundum crystals. They represent a variety of trapped melts, melts and crystals, and subsolidus assemblages. Melts and crystals form upon cooling, both prior to eruption and during quenching upon eruption of the basalts that host the xenoliths [26]. The crystallization of Fe-free phases from silicate melt(s) is due to the immiscible separation of melts from the coexisting silicate melt under highly reducing conditions. Multiple stages of immiscibility, as well as the chemistry and evolution of these melts, are reported in [26]; like yeite (TiSi [5]), toledoite adds more detail to this picture.

Toledoite (TiFeSi) corresponds to the τ_2 phase of [24] in their description of the Fe-Ti-Si system at atmospheric pressures. It melts congruently above 1923 K, but crystallizes from a wide range of melts over a large T range; the temperatures on the Fe-Si side of the ternary are lower than those on the Ti-Si side (Figure 5). This makes toledoite a key phase in the

evolution of low-Si Fe-Ti-Si melts. It can coexist with numerous solid and melt phases and controls the initial fractional crystallization of much of the Fe-Ti-Si system; it is responsible for much mineralogical diversity in the examples from Mount Carmel.

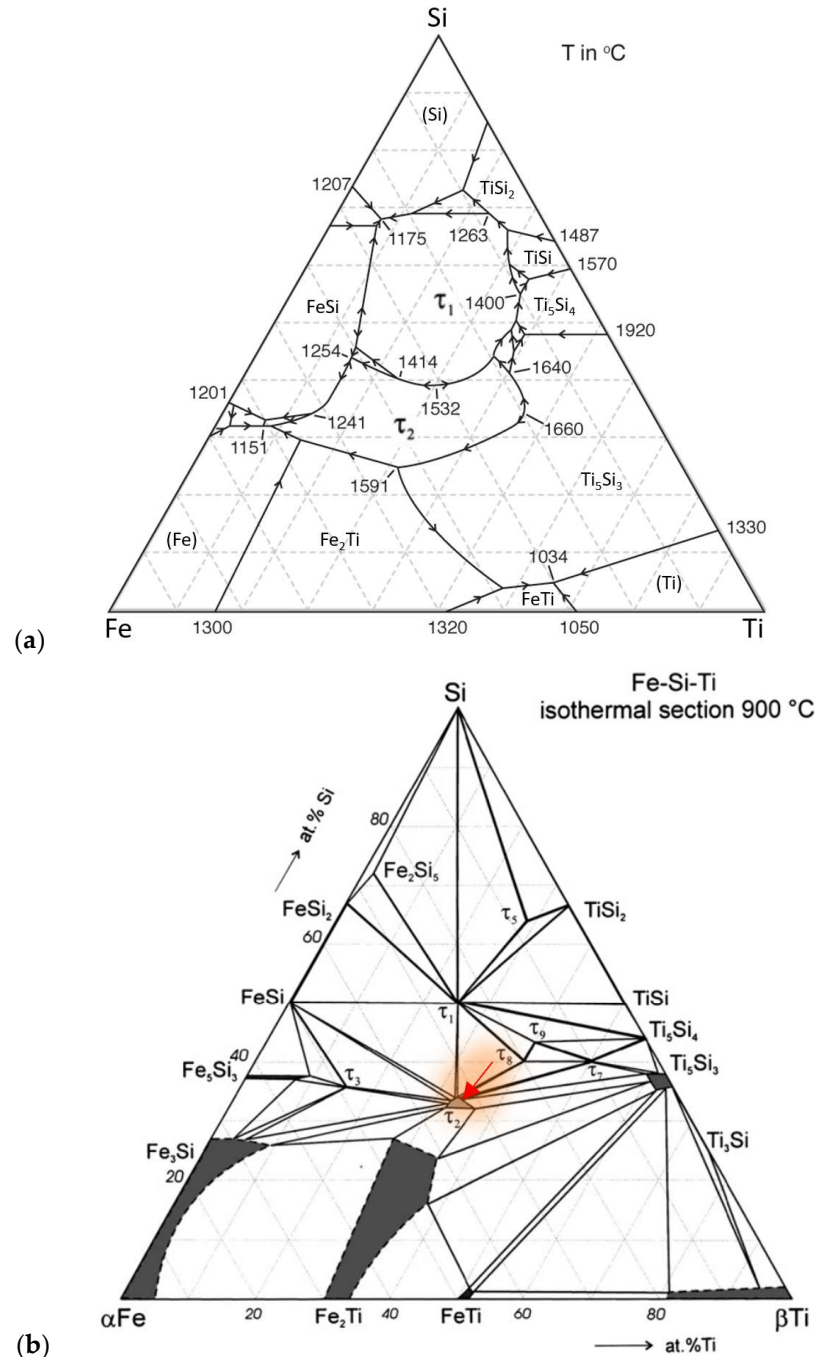


Figure 5. (a) Liquidus projection for Fe-Si-Ti, modified from [24]. (b) Fe-Si-Ti isothermal section for 900 °C from [24]. Red arrow shows composition of toledoite.

Toledoite can occur in two associations (Figure 2): (1) with osbornite (Ti(N,O)), jingsuite (TiB_2), and gupeiite (Fe_3Si); and (2) in spheroidal melt inclusions intimately intergrown with xifengite, naquite, and khamrabaevite (TiC). The first association seems to have formed from a boron-rich silicide melt in equilibrium with an osbornite melt favoring the crystallization of toledoite, gupeiite and jingsuite. Gupeiite does not form directly from a melt in the Fe-Ti-Si ternary but appears in a peritectic reaction ($L + \text{Fe}_2\text{Ti} = \tau_2 + \text{Fe}_3\text{Si}$; 1433 K) and coexists

with toledoite in the subsolidus below 1373 K. This could indicate that the original melt first crystallized Fe₂Ti, and the present assemblage reflects the peritectic assemblage.

The relationships among phases in assemblage (2) suggest that TiC crystallized from a complex Fe-Ti-Si melt, which first crystallized TiC, then broke down into the three silicide phases. However, the assemblage $\tau_2 + \text{Fe}_5\text{Si}_3 + \text{FeSi}$ does not appear in the liquid lines of descent in the Fe-Ti-Si ternary of [24]. In the subsolidus system at 1173–1273 K, toledoite can coexist in equilibrium with either xifengite or naquite, but not with both, and xifengite and naquite do not coexist. The detailed history of this assemblage is therefore not clear.

The wide range of immiscible melt compositions and crystallization conditions captured in the xenoliths from Mount Carmel is shown by these alloy minerals. Therefore, they add some new insights into the processes occurring in a highly reduced magmatic system. Far from being a one-locality oddity, this highly reduced corundum-related assemblage is very similar to other associations that have been already reported from chromitites described in the Luobusa ophiolite in SE Tibet [27,28], and from many other localities in intraplate and subduction-zone tectonic settings [4,26]. A significant role for mantle-derived CH₄+H₂ fluids in magmatic processes is deduced from these occurrences.

Icosahedral quasicrystalline alloys have been described in the Ti-Fe-Si system [29]. The icosahedral phase in this system is stable in a narrow compositional range around Ti₇₀Fe₂₄Si₆. For comparison to the icosahedral quasicrystal, the composition of toledoite based on 100 atoms is Ti₂₈Fe₃₂Si₃₃ with minor Mn, Cr, V and P, making it quite far from the theoretical composition of an icosahedral quasicrystal. Nonetheless, it should be kept in mind that a wide relative variation in the Ti/(Fe+Si) ratio has been observed among the reduced alloy phases in the corundum grains from Mount Carmel [4]. This implies that the Israeli rocks could be the right place to search for the first quasicrystal of terrestrial origin.

5. Conclusions

Toledoite (TiFeSi) is a new alloy mineral that has been discovered in melt inclusions in corundum xenocrysts coming from the Mount Carmel area, Israel. Its chemical composition and crystal structure match those of the synthetic analogue identified by EPMA and EBSD data. Many physical properties cannot be obtained because of its small size, although the data here reported are sufficient to support the correct identification. Toledoite formed under extremely reduced conditions occurring in the upper mantle. It is found in several distinct mineral assemblages and provides more insights into the natural origin of super-reduced mineral phases. The overall mineral associations imply that the low oxygen fugacity of its formation was produced by the interaction of mantle-derived CH₄-H₂ fluids with syenitic melts produced by extreme fraction of mantle-derived mafic melts.

Author Contributions: Conceptualization, C.M., F.C., L.B. and W.L.G.; Methodology, C.M.; Formal analysis, C.M., F.C., L.B. and W.L.G.; Investigation, C.M., F.C., L.B. and W.L.G.; Data curation, C.M.; Writing—original draft, C.M.; Writing—review & editing, C.M., F.C., L.B. and W.L.G. All authors have read and agreed to the published version of the manuscript.

Funding: The research was funded by the MIUR-PRIN2017 project “TEOREM deciphering geological processes using Terrestrial and Extraterrestrial ORE Minerals”, prot. 2017AK8C32 (PI: Luca Bindi).

Data Availability Statement: Data are contained within the article.

Acknowledgments: SEM: EBSD and EPMA analyses were carried out at the Caltech GPS Division Analytical Facility, which is supported, in part, by NSF Grants EAR-0318518 and DMR-0080065. This is contribution 1778 from the ARC Centre of Excellence for Core to Crust Fluid Systems (www.ccfsc.mq.edu.au (accessed on 16 November 2023)) and 1546 from the GEMOC Key Centre (www.gemoc.mq.edu.au (accessed on 16 November 2023)).

Conflicts of Interest: The authors declare no conflicts of interest.

References

1. Kaminsky, F. Mineralogy of the lower mantle: A review of “super-deep” mineral inclusions in diamond. *Earth Sci. Rev.* **2012**, *110*, 127–147. [[CrossRef](#)]
2. Trumbull, R.; Yang, J.-S.; Robinson, P.; Di Pierro, S.; Vennemann, T.; Wiedenbeck, M. The carbon isotope composition of natural SiC (moissanite) from the Earth’s mantle: New discoveries from ophiolites. *Lithos* **2009**, *113*, 612–620. [[CrossRef](#)]
3. Dobrzynetskaia, L.; Mukhin, P.; Wang, Q.; Wirth, R.; O’ Bannon, E.; Zhao, W.; Eppelbaum, L.; Sokhonchuk, T. Moissanite (SiC) with metal-silicide and silicon inclusions from tuff of Israel: Raman spectroscopy and electron microscope studies. *Lithos* **2018**, *310–311*, 355–368. [[CrossRef](#)]
4. Griffin, W.L.; Bindi, L.; Cámara, F.; Ma, C.; Gain, S.E.M.; Saunders, M.; Alard, O.; Huang, J.-X.; Shaw, J.; Meredith, C.; et al. Interactions of magmas and highly reduced fluids during intraplate volcanism, Mt Carmel, Israel: Implications for mantle redox states and global carbon cycles. *Gondwana Res.* **2024**, *128*, 14–54. [[CrossRef](#)]
5. Ma, C.; Cámara, F.; Bindi, L.; Toledo, V.; Griffin, W.L. New minerals from inclusions in corundum xenocrysts from Mt Carmel, Israel: Magnéliite, ziroite, sassite, mizraite-(Ce) and yeite. *Materials* **2023**, *16*, 7578. [[CrossRef](#)]
6. Ma, C.; Beckett, J.R. Kaitianite, $\text{Ti}^{3+}_2\text{Ti}^{4+}\text{O}_5$, a new titanium oxide mineral from Allende. *Meteorit. Planet. Sci.* **2021**, *56*, 96–107. [[CrossRef](#)]
7. Litasov, K.D.; Bekker, T.B.; Kagi, H. Reply to the discussion of “Enigmatic superreduced phases in corundum from natural rocks: Possible contamination from artificial abrasive materials or metallurgical slags” by Litasov et al. (Lithos, v.340–341, p.181–190) by W.L. Griffin, V. Toledo and S.Y. O’Reilly. *Lithos* **2019**, *348–349*, 105170.
8. Litasov, K.D.; Kagi, H.; Bekker, T.B. Enigmatic super-reduced phases in corundum from natural rocks: Possible contamination from artificial abrasive materials or metallurgical slags. *Lithos* **2019**, *340–341*, 181–190. [[CrossRef](#)]
9. Ballhaus, C.; Helmy, H.M.; Fonseca, R.O.C.; Wirth, R.; Schreiber, A.; Jöns, N. Ultra-reduced phases in ophiolites cannot come from the Earth’s mantle. *Am. Mineral.* **2021**, *106*, 1053–1063. [[CrossRef](#)]
10. Galuskin, E.; Galuskina, I. Evidence of the antoropogenic origin of the “Carmel Sapphire” with enigmatic super-reduced minerals. *Min. Mag.* **2023**, *87*, 619–630. [[CrossRef](#)]
11. Galuskin, E.; Galuskina, I. Reply to the discussion of “Evidence of the anthropogenic origin of the ‘Carmel sapphire’ with enigmatic super-reduced minerals” by E. Galuskin and I. Galuskina (Mineralogical Magazine, 87, 631–634) by W.L. Griffin, V. Toledo and S.Y. O’Reilly. *Min. Mag.* **2023**, *87*, 635–638. [[CrossRef](#)]
12. Griffin, W.L.; Toledo, V.; O’Reilly, S.Y. Discussion of “Enigmatic super-reduced phases in corundum from natural rocks: Possible contamination from artificial abrasive materials or metallurgical slags” by Litasov et al. *Lithos* **2019**, *348–349*, 105122. [[CrossRef](#)]
13. Griffin, W.L.; Toledo, V.; O’Reilly, S.Y. Discussion of paper by Galuskin and Galuskina, “Evidence of the anthropogenic origin of the “Carmel Sapphire” with enigmatic super-reduced minerals”. *Min. Mag.* **2023**, *87*, 631–634. [[CrossRef](#)]
14. Griffin, W.L.; Gain, S.E.M.; Huang, J.-X.; Belousova, E.A.; Toledo, V.; O’Reilly, S.Y. Permian to Quaternary magmatism beneath the Mt Carmel area, Israel: Zircons from volcanic rocks and associated alluvial deposits. *Lithos* **2018**, *314–315*, 307–322. [[CrossRef](#)]
15. Yu, Z. Two new minerals gupeite and xifengite in cosmic dusts from Yanshan. *Acta Petrol. Mineral. Et Anal.* **1984**, *3*, 231–238.
16. Xiong, F.; Xu, X.; Mugnaioli, E.; Gemmi, M.; Wirth, R.; Grew, E.S.; Robinson, P.T. Jingsuiite, TiB_2 , a new mineral from the Cr-11 podiform chromitite orebody, Luobusa ophiolite, Tibet, China: Implications for recycling of boron. *Am. Mineral.* **2022**, *107*, 43–53. [[CrossRef](#)]
17. Story-Maskelyne, M.H.N.X. On the mineral constituents of meteorites. *Phil. Trans. R. Soc.* **1870**, *160*, 189–214.
18. Shi, N.; Bai, W.; Li, G.; Xiong, M.; Yang, J.; Ma, Z.; Rong, H. Naquite, FeSi , a new mineral species from Luobusha, Tibet, Western China. *Acta Geol. Sin.* **2012**, *86*, 533–538.
19. Jeitschko, W. The crystal structure of TiFeSi and related compounds. *Acta Crystallogr. B Struct. Crystallogr. Cryst. Chem.* **1970**, *26*, 815–822. [[CrossRef](#)]
20. Baur, W.H. The Geometry of Polyhedral Distortions. Predictive Relationships for the Phosphate Group. *Acta Crystallogr. B Struct. Crystallogr. Cryst. Eng. Mater.* **1974**, *30*, 1195–1215. [[CrossRef](#)]
21. Li, G.; Fang, Q.; Shi, N.; Bai, W.; Yang, J.; Xiong, M.; Ma, Z.; Rong, H. Zangboite, TiFeSi_2 , a new mineral species from Luobusha, Tibet, China, and its crystal structure. *Can. Mineral.* **2009**, *47*, 1265–1274.
22. Momma, K.; Izumi, F. VESTA 3 for three-dimensional visualization of crystal, volumetric and morphology data. *J. Appl. Crystallogr.* **2011**, *44*, 1272–1276. [[CrossRef](#)]
23. Wolfgang, J. Ternary phases with TiFeSi and ordered Fe_2P type structures. *Metall. Trans.* **1970**, *1*, 2963–2965.
24. Weitzer, F.; Schuster, J.C.; Naka, M.; Stein, F.; Palm, M. On the reaction scheme and liquidus surface in the ternary system Fe-Si-Ti. *Intermetallics* **2008**, *16*, 273–282. [[CrossRef](#)]
25. Marshall, M.; Sanford, J.; Shelton, W.; Xie, W. The crystal structures and magnetic properties of TiFeSi coexisting in hexagonal and orthorhombic symmetries. *J. Alloys Compd.* **2021**, *864*, 158617. [[CrossRef](#)]
26. Griffin, W.L.; Gain, S.E.M.; Saunders, M.; Huang, J.-X.; Alard, O.; Toledo, V.; O’Reilly, S.Y. Immiscible metallic melts in the upper mantle beneath Mount Carmel, Israel: Silicides, phosphides and carbides. *Am. Mineral.* **2022**, *107*, 532–549. [[CrossRef](#)]
27. Xiong, F.; Xu, X.; Mugnaioli, E.; Gemmi, M.; Wirth, R.; Grew, E.S.; Robinson, P.T.; Yang, J. Two new minerals, badengzhuite, TiP , and zhiqinite, TiSi_2 , from the Cr-11 chromitite orebody, Luobusa ophiolite, Tibet, China: Is this evidence for super-reduced mantle-derived fluids? *Eur. J. Mineral.* **2020**, *32*, 557–574. [[CrossRef](#)]

28. Xiong, F.; Xu, X.; Mugnaioli, E.; Gemmi, M.; Wirth, R.; Yang, J.; Grew, E.S. Wenjiite, $Ti_{10}(Si,P,\square)_7$, and kangjinlaite, $Ti_{11}(Si,P)_{10}$, new minerals in the ternary Ti-P-Si system from the Luobusa ophiolite, Tibet, China. *Am. Mineral.* **2023**, *108*, 197–210. [[CrossRef](#)]
29. Mandal, P. Structural disorder in Ti-Fe-Si icosahedral quasicrystal. *J. Alloys Compd.* **2003**, *361*, 96–101. [[CrossRef](#)]

Disclaimer/Publisher's Note: The statements, opinions and data contained in all publications are solely those of the individual author(s) and contributor(s) and not of MDPI and/or the editor(s). MDPI and/or the editor(s) disclaim responsibility for any injury to people or property resulting from any ideas, methods, instructions or products referred to in the content.